GEOLOGIJA 68/2, 269-286, Ljubljana 2025

https://doi.org/10.5474/geologija.2025.012

Article

Petrography and geothermobarometry of quartz diorite from Pohorje Mountains, Slovenia

Petrografija in geotermobarometrija kremenovega diorita s Pohorja

Tim SOTELŠEK[1], Simona JARC[1], Andreja PAJNKIHER[2] & Mirijam VRABEC[1]*

[1]University of Ljubljana, Faculty of Natural Sciences and Engineering, Department of Geology, Aškerčeva cesta 12, SI-1000 Ljubljana, Slovenia; e-mail: tim.sotelsek@ntf.uni-lj.si; simona.jarc@ntf.uni-lj.si;
*corresponding author: mirijam.vrabec@ntf.uni-lj.si
[2]ELEA IC projektiranje in svetovanje, Dunajska cesta 21, SI-1000 Ljubljana, Slovenia; e-mail: andreja.pajnkiher@gmail.com

Prejeto / Received 5. 9. 2025; Sprejeto / Accepted 21. 11. 2025; Objavljeno na spletu / Published online 10. 12. 2025

Key words: quartz diorite, "cizlakite", petrography, clinopyroxene geothermobarometry, amphibole geothermobaromery, amphibole–plagioclase thermometry, Pohorje Mountains
Ključne besede: kremenov diorit, "čizlakit", petrografija, klinopiroksenova geotermobarometrija, amfibolova geobarometrija, amfibol–plagioklaz termometrija, Pohorje

Abstract

The mineral composition and pressure–temperature conditions of Pohorje quartz diorite were investigated to reconstruct crystallization sequence and integrate the results with previous data on the Pohorje igneous complex, providing insights into its petrogenesis. Pohorje quartz diorite has phaneritic texture and is medium- to coarse-grained. The major minerals include light green clinopyroxene, dark green amphiboles, and white feldspars; the first two give the rock its characteristic colour. The proportion of dark- to light-colored minerals is approximately 4:1. Clinopyroxene predominates and correspond to diopside (X_{Ca} = 0.47–0.51, X_{Mg} = 0.41–0.49, X_{Fe} = 0.05–0.09). Amphiboles are Ca-amphiboles and are divided into two types: Type I amphiboles occur as single grains with distinctive core and rim zones, whereas Type II amphiboles replace clinopyroxene grains. Type I amphibole cores are classified as magnesiohornblende, tschermakite, edenite, pargasite, or magnesiohastingsite; Type I amphibole rims are classified as magnesiohornblende and actinolite; and Type II amphiboles are classified as magnesiohornblende. The dominant feldspars are oligoclase to andesine (X_{Ab} = 0.61–0.73), often replaced by potassium feldspar orthoclase. Minor minerals include quartz, biotite group minerals, apatite group minerals, titanite, epidote group minerals (allanite), and magnetite, while secondary minerals comprise chlorite group minerals and calcite. Various thermometers and barometers were applied to reconstruct the crystallization history of the quartz diorite and link it to the evolution of the host granodiorite intrusion. Thermobarometric data indicate that clinopyroxene in the quartz diorite, which is considered the earliest cumulate product from basaltic melts, crystallized under the highest P–T conditions (840–905 °C; 6.70–7.70 kbar), consistent with petrographic evidence. Subsequent crystallization of Type I amphibole cores occurred at 675–730 °C and 6.45–6.50 kbar, conditions comparable to those of the less evolved granodiorite, suggesting coeval formation. Later stages involved the formation of Type I amphibole rims at 585–640 °C and ~2.00 kbar, Type II amphiboles at 615–680 °C and 2.59–2.79 kbar, and biotites at 670–690 °C, associated with the emplacement of more evolved granodiorite at shallower crustal levels.

Izvleček

Proučili smo mineralno sestavo in tlačno-temperaturne pogoje nastanka pohorskega kremenovega diorita, z namenom določitve zaporedja kristalizacije posameznih mineralov. Dobljene rezultate smo povezali z objavljenimi podatki o pohorski granodioritni intruziji, kar omogoča dodaten vpogled v petrogenzo kremenovega diorita. Pohorski kremenov diorit ima faneritsko strukturo in je srednje do debelozrnat. Glavne minerale predstavljajo svetlozeleni klinopirokseni in temnozeleni amfiboli, ki dajo kamnini značilno barvo, ter beli glinenci. Razmerje med temnimi in svetlimi minerali je približno 4:1. V kamnini prevladuje klinopiroksen, ki ustreza diopsidu (X_{Ca} = 0,47–0,51, X_{Mg} = 0,41–0,49, X_{Fe} = 0,05–0,09). Amfiboli so Ca-amfiboli in jih lahko razdelimo na dve vrsti: amfiboli tipa I se pojavljajo kot posamezna zrna z značilno različno sestavo jedra in robnih delov, medtem ko amfiboli tipa II nadomeščajo zrna klinopiroksenov. Jedra amfibolov tipa I pripadajo magnezijski-rogovači, tschermakitu, edenitu, pargasitu ali magneziohastingsitu; robni deli amfibolov tipa I pripadajo magnezijski-rogovači in aktinolitu; amfiboli tipa II so po klasifikaciji vsi magnezijska-rogovača. Med glinenci prevladujejo plagioklazi sestave oligoklaz do andezin (X_{Ab} = 0,61–0,73), ki so pogosto nadomeščeni z ortoklazom. Med manj zastopanimi minerali se pojavljajo kremen, biotiti, apatiti, titanit, minerali epidotove skupine (allanit) in magnetit, od sekundarnih mineralov so prisotni kloriti in kalcit. Da bi rekonstruirali zgodovino kristalizacije kremenovega diorita in ga povezali z razvojem glavnega granodioritnega intruziva smo uporabili različne geotermometre in geobarometre. Rezultati geotermobarometrije kažejo, da so klinopirokseni v kremenovem dioritu, ki velja za najzgodnejši kumulat bazaltnih talin, kristalili pri najvišjih P–T pogojih (840–905 °C; 6,70–7,70 kbar), kar je skladno s petrografskimi dokazi. Sledila je kristalizacija jeder amfibolov tipa I, ki je potekala pri 675–730 °C in 6,45–6,50 kbar, kar ustreza pogojem kristalizacije manj razvitega granodiorita in nakazuje njihov sočasni nastanek. Kasnejše faze so vključevale nastanek robnih delov amfibolov tipa I pri 585–640 °C in ~2,00 kbar, amfibolov tipa II pri 615–680 °C in 2,59–2,79 kbar, ter biotitov pri 670–690 °C in so povezane z intruzijo bolj razvitega granodiorita v višje nivoje skorje.

Introduction

Quartz diorite, in the past also known as "cizlakite" is an intrusive igneous rock. It consists of dark green amphiboles, light green pyroxene, white feldspars and quartz, with minor biotite group minerals (in continuation biotite), titanite, epidote group minerals (allanite), apatite group minerals (in continuation apatite), chlorite group minerals (in continuation chlorite), calcite and opaque minerals, mainly magnetite. In Slovenia, it occurs in only one location – on Pohorje, near the village of Cezlak, forming large enclave within granodiorite host rock. In the past, both granodiorite and quartz diorite were extracted. The quarry of quartz diorite had a significant economic value for the natural stone industry and at the same time represents an important natural heritage site (ARSO, 2018).

The first studies of the igneous rocks of Pohorje were carried out by Benesch (1917). He drew attention to a smaller outcrop of "green stone", analysed it and described it as quartz hornblende augite diorite, and thus classified it as diorite. Dolar-Mantuani (1935) analysed samples of quartz diorite, which were subsequently named by Nikitin & Klemen (1937) as tylaite, a rock with a transitional composition between gabbro and peridotite. Nikitin & Klemen (1937) described quartz diorite more precisely as a quartz hornblende augite diorite containing 70–80% mafic minerals (hornblende, augite, biotite, apatite, titanite) and 20–30% salic minerals (quartz, plagioclases). As the existing name was not suitable, Nikitin (1939) carried out a detailed classification and defined the rock as a separate igneous rock according to the CIPW system, which he named "cizlakite" after the village of Čizlak (now Cezlak). Rock was considered as a product of the early gravitational differentiation during crystallization of granodioritic magma (Nikitin & Klemen, 1937; Nikitin, 1939; Faninger, 1965).

Later investigations confirmed the characteristic mineral composition with dominant augite, hornblende and an anorthite component in the plagioclases between 34 and 52% (Dolar-Mantuani, 1935, 1940; Nikitin, 1939; Faninger, 1973). Faninger (1973) suggested that quartz diorite is a product of hybridisation of ultramafic magma with magma from the Pohorje main igneous rock, while Dolenec et al. (1987) concluded, that quartz diorite is classified as a gabbroic rock based on the isotopic composition of oxygen. Činč (1992) showed that quartz diorite was formed by fractional crystallization of tholeiitic magma and that the samples fall into the gabbro or quartz gabbro field according to Streckeisen's classification. Dolenec (1994) determined the Miocene age of the quartz diorite (18.7 ±0.7 Ma) using the radiometric K–Ar method, confirming that it is slightly older than granodiorite, which Nikitin (1939) had already surmised. Poli et al. (2020) claimed that mixing and fractional crystallization were responsible for the formation of rocks from the Pohorje Igneous Complex (PIC) including granodiorite, tonalite and quartz diorite. The geodynamic sequence involves mantle metasomatism, crustal thickening, and mantle melt production in response to tectonic events.

The objective of this study is to characterize the mineral composition of quartz diorite and to reconstruct the crystallization sequence and pressure–temperature conditions using optical microscopy, cold cathodoluminescence, electron microprobe analysis, and geothermobarometric calculations. The results are integrated with previously published data on the Pohorje igneous complex to provide a more comprehensive understanding of its petrogenesis.

Geological setting

Pohorje is part of the Eastern Alps, which consist of Cretaceous nappes, collectively known as the Austroalpine nappes, or Austroalpine for short. The Eastern Alps include Kobansko, Pohorje, the northern Karawanke, and Strojna. The Pohorje Mountains are bounded to the west and southwest by the Labot Fault, which separates them from the Southern Alps; to the north, the Ribnica trough separates them from the lithologically similar structures of Strojna and Kozjak; and to the east and southeast, they sink beneath the Plio–Quaternary sediments of the Pannonian Basin (Fig. 1) (Mioč, 1978; Mioč & Žnidarčič, 1989).

The sequence of Cretaceous nappes in Pohorje begins with the structurally deepest Pohorje nappe, composed of medium to high metamorphic rocks. This is followed by two further nappes, namely the first, structurally higher nappe with low-grade metamorphic rocks, mainly schists and phyllites, and the second nappe composed of clastic sedimentary rocks (Janák et al., 2004). The entire sequence is overlain by Miocene sediments of the Pannonian Basin (Fodor et al., 2003, 2008).

The metamorphic rocks from the Pohorje nappe are mainly gneisses, and, less commonly, micaschist, containing lenses of eclogite, amphibolite, marble, quartzite, and a somewhat larger ultrabasic body with remnants of garnet peridotite (Hinterlechner-Ravnik, 1971, 1973; Hinterlechner-Ravnik & Moine, 1977; Hinterlechner-Ravnik

et al., 1991a, b) (Fig. 1a). These rocks underwent intracontinental subduction during the Cretaceous orogeny, descending to depths over 100 km (Janák et al., 2004). At these depths, they experienced ultrahigh pressure metamorphic conditions at pressures up to 4.0 GPa and temperatures of 750–940 °C (e.g., Vrabec et al., 2012; Janák et al., 2015).

The Pohorje nappe is folded into an antiform (Pohorje antiform; Kirst et al., 2010), with an axis trending east–southeast to west–northwest. Its central part is occupied by the Pohorje Igneous Complex (Poli et al., 2020), which intruded metamorphic rocks during the Miocene (ca. 18 Ma; Zupančič, 1994; Altherr et al., 1995; Fodor et al., 2008; Trajanova et al., 2008). The PIC comprises three main rock groups: (1) granodiorite, tonalite (GDT), and quartz diorite; (2) dacite dykes and stocks intruding both metamorphic rocks and GDT, particularly in western Pohorje, together with porphyritic microgranodiorite (DAMG); and (3) andesitic dykes (AD), which mainly cut metamorphic rocks and less commonly GDT (Poli et al., 2020). Magmatic activity in the PIC occurred in multiple pulses (Poli et al., 2020). The first pulse (ca. 20 Ma) involved the ascent of small mafic magma batches to middle-crustal level chambers, where cumulus processes produced the quartz diorite body. During the second pulse (ca. 18 Ma, 6.2 kbar), hybridized magmas rose into middle-crustal level chambers and crystallized to form less evolved GDT that enclosed the earlier quartz diorite. Continued magma–felsic interaction during the third pulse (ca. 17 Ma, 4.2 kbar) generated more evolved GDT, with chamber depths decreasing in response to rapid uplift. The fourth pulse (ca. 16 Ma, 2–3 kbar) was characterized by magmas that evolved through mixing and fractional crystallization (MFC), ascended into subvolcanic-level chambers, and were emplaced as Ga-rich DAMG dykes and sheet-like intrusions. The fifth pulse (ca. 17 Ma) introduced small batches of mantle-derived melts into middle-crustal levels, producing dykes and crosscutting intrusions of Ga-poor DAMG. In the final stages of crystallization, residual granitic melts (~20%) intruded GDT and quartz diorite as aplitic and pegmatitic bodies, cutting the main intrusion in multiple directions; these late-stage intrusions occur both at the pluton margins and, locally, within the surrounding metamorphic rocks (Poli et al., 2020).

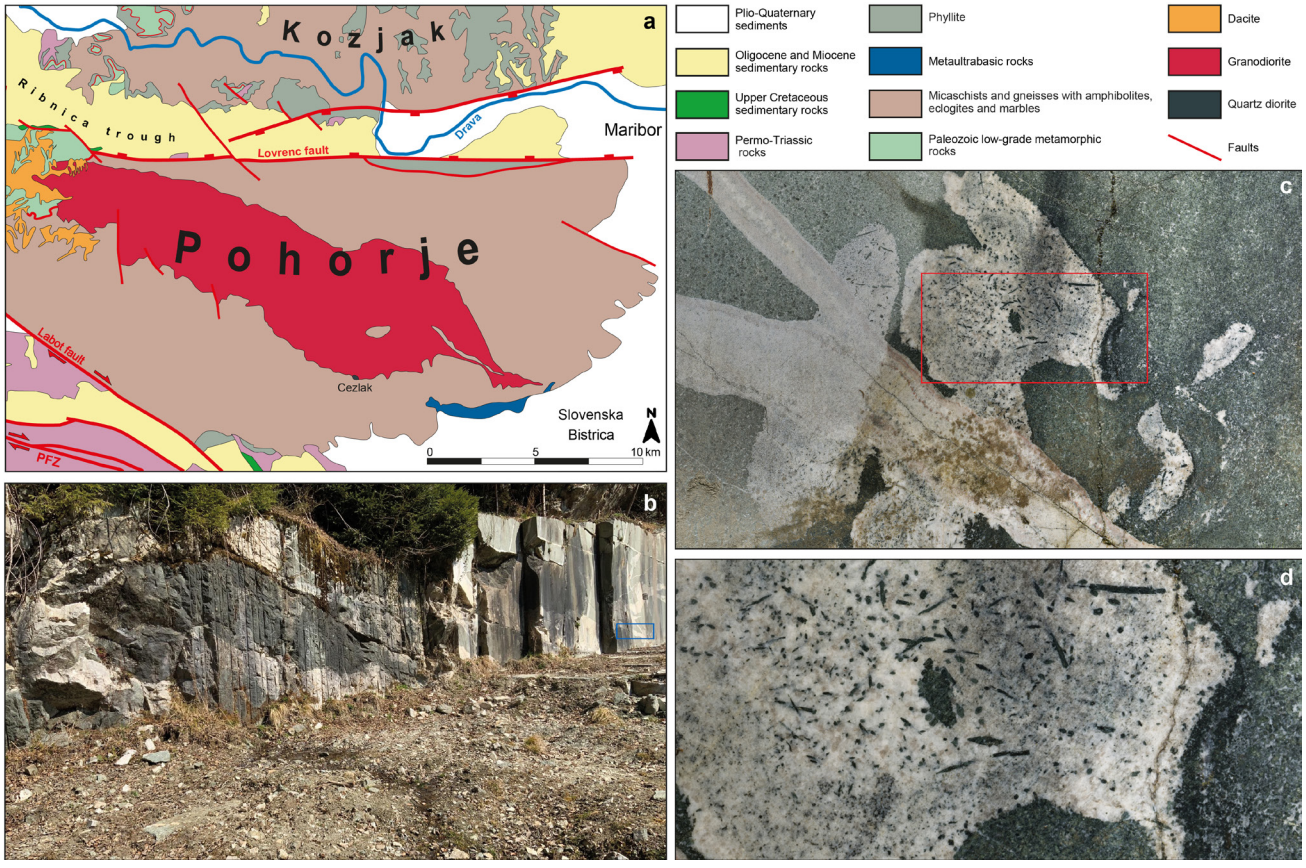

Fig. 1. (a) Simplified geological map showing the position of the quartz diorite body (modified after Mioč & Žnidarčič, 1977). (b) Present-day view of the Cezlak II quarry. (c) Close-up of a quarry wall section, where pegmatite veins clearly cutting through the quartz diorite (marked with a blue rectangle in panel b). (d) Elongated amphibole crystals (up to 5 cm) visible within the pegmatite vein (marked with a red rectangle in panel c).

Table 1. List of quartz diorite samples from Cezlak II quarry.

Sample number	Sample description	Thin section number
C1	Quartz diorite	C1-1
C2	Quartz diorite	C2-1
C3	Quartz diorite	C3-1, C3-2, C3-3, C3-4
C4	Quartz diorite in contact with pegmatite vein	C4-1
C5	Quartz diorite in contact with pegmatite vein	C5-1, C5-2
C6	Quartz diorite in contact with pegmatite vein	C6-1, C6-2
C7	Quartz diorite in contact with pegmatite vein	C7-1, C7-2, C7-3
C8	Quartz diorite in contact with pegmatite vein	C8-1, C8-2, C8-3
C9	Quartz diorite	C9-1
C10	Quartz diorite	C10-1

Sotelšek (2019) determined pressures and temperatures of granodiorite intrusion using conventional amphibole and biotite geothermobarometers. Calculated pressures decrease from southeast to northwest from 6.6 kbar to 2 kbar, suggesting that the intrusion was tilted after emplacement. Temperatures follow the same decreasing trend from 724 °C in the southeast to 670 °C in the northwest.

Materials and methods

Samples and sample preparations

Available fresh rock samples were collected in the abandoned Cezlak II quarry (Fig. 1b), from which 19 thin sections were prepared. The samples, thin sections, and corresponding labels are presented in Table 1.

Optical microscopy

Polished thin sections were examined with a Nikon Eclipse E200 optical polarising microscope. A Nikon DS-Fi1 camera and the NIS-Elements Basic Research software were used for photo documentation of individual areas under parallel and crossed polars. A method of point counting was used to determine the relative proportions between minerals in thin sections. Between 400 and 600 points were counted per sample, depending on the grain size and texture.

Optical cathodoluminescence with cold cathode

Cathodoluminescence (CL) imaging was performed on polished thin sections of selected samples in order to examine mineral textures, zoning, and phase relations. The measurements were conducted using a CITL 8200 Mk3 cold-cathode CL stage attached to an Olympus BH2 petrographic microscope. Analytical conditions were kept stable, with a vacuum of ~0.05–0.1 mbar, an accelerating voltage of 14–15 kV, and a beam current of 200–300 μA.

Images were captured using a digital camera under constant operating parameters to ensure comparability between minerals. With this method, clear distinction between potassium feldspar, plagioclases, quartz, amphiboles, and accessory phases such as apatite, was possible based on their characteristic luminescence colours. Luminescence colours were used qualitatively to recognize textural features and were processed only for brightness and contrast adjustment, without modification of the original colour information.

Electron microprobe analyses (EPMA) with wavelength dispersive spectroscopy (WDS)

Electron microprobe analyses (EPMA) with wavelength dispersive spectroscopy (WDS) were carried out using a CAMECA SX-100 microprobe, operating at an electron acceleration voltage of 15 kV, a beam current of 20 nA, and a peak counting time of 20 s. All analyses were spot measurements using an electron beam with cross-section of 5 μm. Raw counts were corrected using a PAP routine. A total of 45 amphibole grains, 30 clinopyroxene grains, 30 plagioclase grains, 20 potassium feldspar grains, and 3–5 grains of minor mineral phases were measured. Within individual grains 4–6 spot measurements were conducted.

The contents of the following oxides were measured: SiO_2, TiO_2, Al_2O_3, Cr_2O_3, Na_2O, K_2O, FeO, MnO, MgO, and CaO, using the following standards: LiF for F, albite for Na, orthoclase for Si, orthoclase for K, Al_2O_3 for Al, NaCl for Cl, wollastonite for Ca, TiO_2 for Ti, fayalite for Fe, rhodonite for Mn, forsterite for Mg, Cr for Cr, and Ni for Ni. The chemical composition of minerals — including clinopyroxene, amphiboles, plagioclases, biotite, potassium feldspar, quartz, chlorite, and

epidote group minerals — was determined on samples C1-1, C3-1, C4-1, C7-3, and C8-3.

Content of Fe^{2+} and Fe^{3+} in amphiboles and pyroxene was determined by stoichiometric calculations. The presented ferric iron content in amphiboles was estimated based on averaged normalization to 15 cations excluding Na, K ((15eNK + 15eK)/2) (Yavuz & Döner, 2017). Where needed, the normalizations were recalculated considering the required calculation steps for the specific thermobarometer. The calculation of ferric iron in pyroxene was determined as the average of Fe^{3+} content calculated using the models of Droop (1987) and Papike et al. (1974). All iron in other minerals was considered as Fe^{2+}.

Geothermobarometric calculations

Pressures and temperatures are key parameters for determining the emplacement sequence of plutons. To constrain the pressure and temperature conditions of quartz diorite crystallization, we applied several geothermobarometers, which are listed in Table 2.

For geothermobarometric calculations involving amphiboles, understanding the specific site-related reactions within the amphibole structure can provide valuable insight. A substitution analysis is commonly used to check for the major substitution types. A Tschermak molecule substitution is thought to be a function of temperature and pressure (Anderson and Smith, 1995; Hammarston and Zen, 1986; Helz, 1982). Al-Tschermak exchange is pressure sensitive and can be written as $^{C}(Mg,Fe) + {}^{T}Si = {}^{VI}Al + {}^{IV}Al$, where Al in tetrahedral coordination (^{IV}Al) replaces ^{T}Si and Al in octahedral coordination (^{VI}Al) replaces Mg and Fe in C sites. Ti-Tschermak exchange is a temperature-sensitive coupled substitution, where ^{C}Ti replaces ^{B}Mg, which leads to ^{T}Si being replaced by ^{IV}Al. At higher temperatures it can be expressed as $^{B}Mg + {}^{T}Si = {}^{C}Ti + {}^{IV}Al$. Another temperature sensitive substitution is edenite substitution written as $^{A}vacancy + {}^{T}Si = {}^{A}(Na + K) + {}^{IV}Al$, where higher $^{A}(Na + K)$ is accommodated by the exchange of ^{T}Si with ^{IV}Al (Helz, 1982; Hammarstrom & Zen, 1986; Anderson & Smith, 1995). Plagioclase substitution can also play an important role in the content of ^{IV}Al in amphiboles as variations in albite and anorthite components in coexisting plagioclase can affect Al incorporation at the T site (Blundy & Holland, 1990; Holland & Blundy, 1994) and can be expressed as $^{B}Na + {}^{T}Si = {}^{B}Ca + {}^{IV}Al$.

Results

Macroscopic description

Quartz diorite has phaneritic structure and is medium- to coarse-grained with a grain size of up to 8 mm (Figure 2a,b). It is heterogeneous both in grain size and in the proportion of individual minerals. It consists of dark green amphiboles, light green pyroxene, white feldspars, and greyish quartz. Visually, the green colour dominates, which is due to the main minerals, pyroxene 4–7 mm in size, and amphiboles up to 8 mm in size. The ratio between the proportion of mafic and salic minerals determined using picture analysis of scanned polished hand specimens is about 4:1 in most cases. Samples are often intersected by pegmatite veins (Fig. 1c,d and Fig. 2c,d). The pegmatite is uniform and medium-grained with a grain size of up to 5 mm. It contains white feldspars, greyish quartz, a small amount of elongated green amphibole minerals occasionally reaching 5 cm in length, calcite and rare beryl.

Table 2. Selected geothermobarometers and their calibrations applied to calculate the P–T conditions of quartz diorite crystallization.

Geothermobarometer	Estimated uncertainty	Reference	Abbreviation
Clinopyroxene barometer	± 1.70 kbar	Nimis & Ulmer (1998)	NU98
Clinopyroxene barometer	± 1.10 kbar	Nimis (1999)	N99
Fe^{2+}–Mg exchange Clinopyroxene thermometer	Not reported	Dal Negro et al. (1982)	DN82
Fe^{2+}–Mg exchange Clinopyroxene thermometer	Not reported	Molin & Zanazzi (1991)	MZ91
Fe^{2+}–Mg exchange Clinopyroxene thermometer	Not reported	Bertrand & Mercier (1985)	BM85
Al-in-Amphibole barometer	± 0.6 kbar	Schmidt (1992)	S92
Al-in-Amphibole barometer	± 0.6 kbar	Anderson & Smith (1995)	AS96
Amphibole–Plagioclase thermometer	± 30 °C	Blundy & Holland (1990)	BH90
Amphibole–Plagioclase thermometer	± 30 °C	Holland & Blundy (1994)	HB94
Ti-in-Amphibole thermometer	± 25 °C	Otten (1984)	O84
Biotite thermometer	± 23 °C	Luhr et al. (1984)	L84
Biotite thermometer	± 24 °C	Henry et al. (2005)	H05

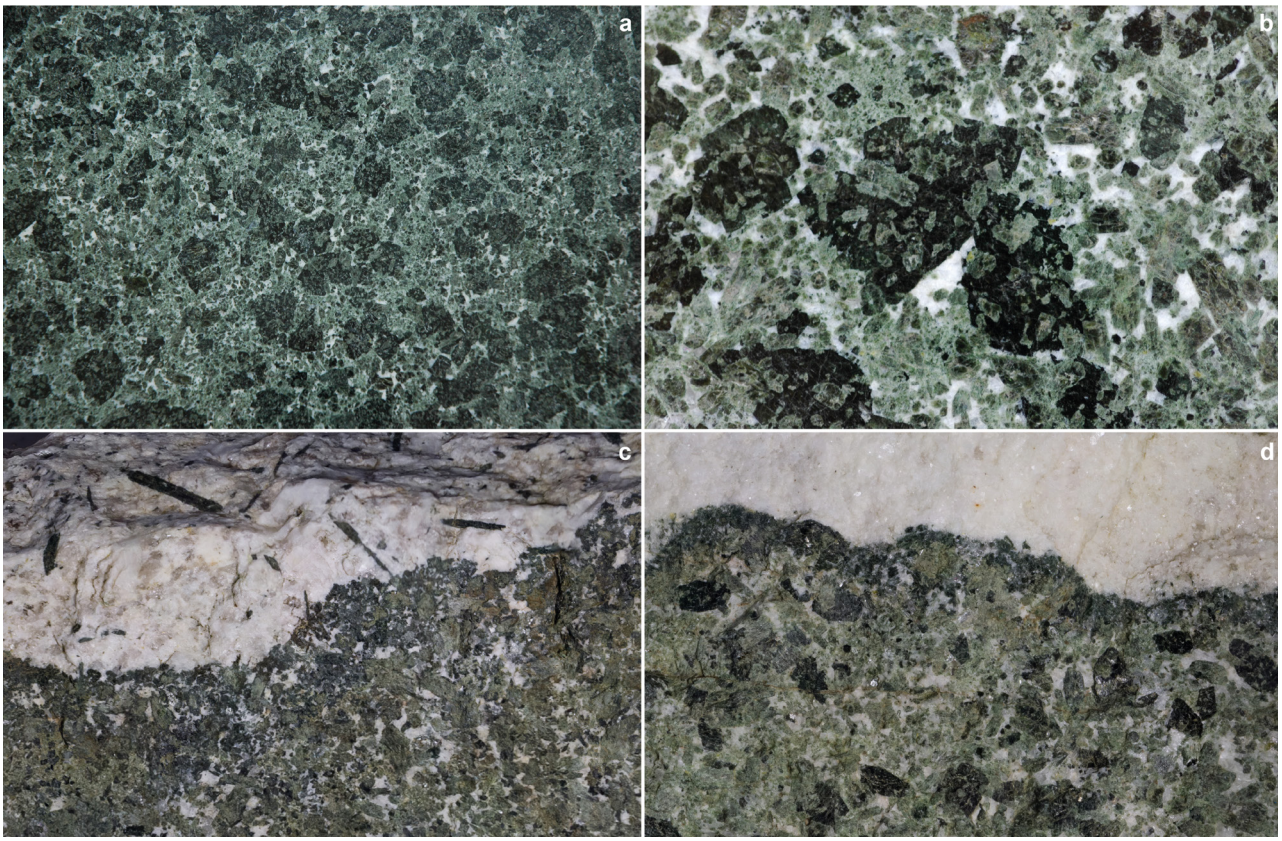

Fig. 2. Close-up of the polished surface of a quartz diorite hand specimens. (a) The prevailing green colour of the rock is a result of the combination of pale green clinopyroxene and dark green amphiboles. (b) Amphibole replacing pyroxene is forming an uralitic structure. The white minerals are feldspars, and the grey mineral (lower left corner) is quartz. (c, d) Samples are often cut by pegmatitic veins, composed of quartz, feldspars and common elongated amphibole grains. The lower border of each picture measures 12 cm.

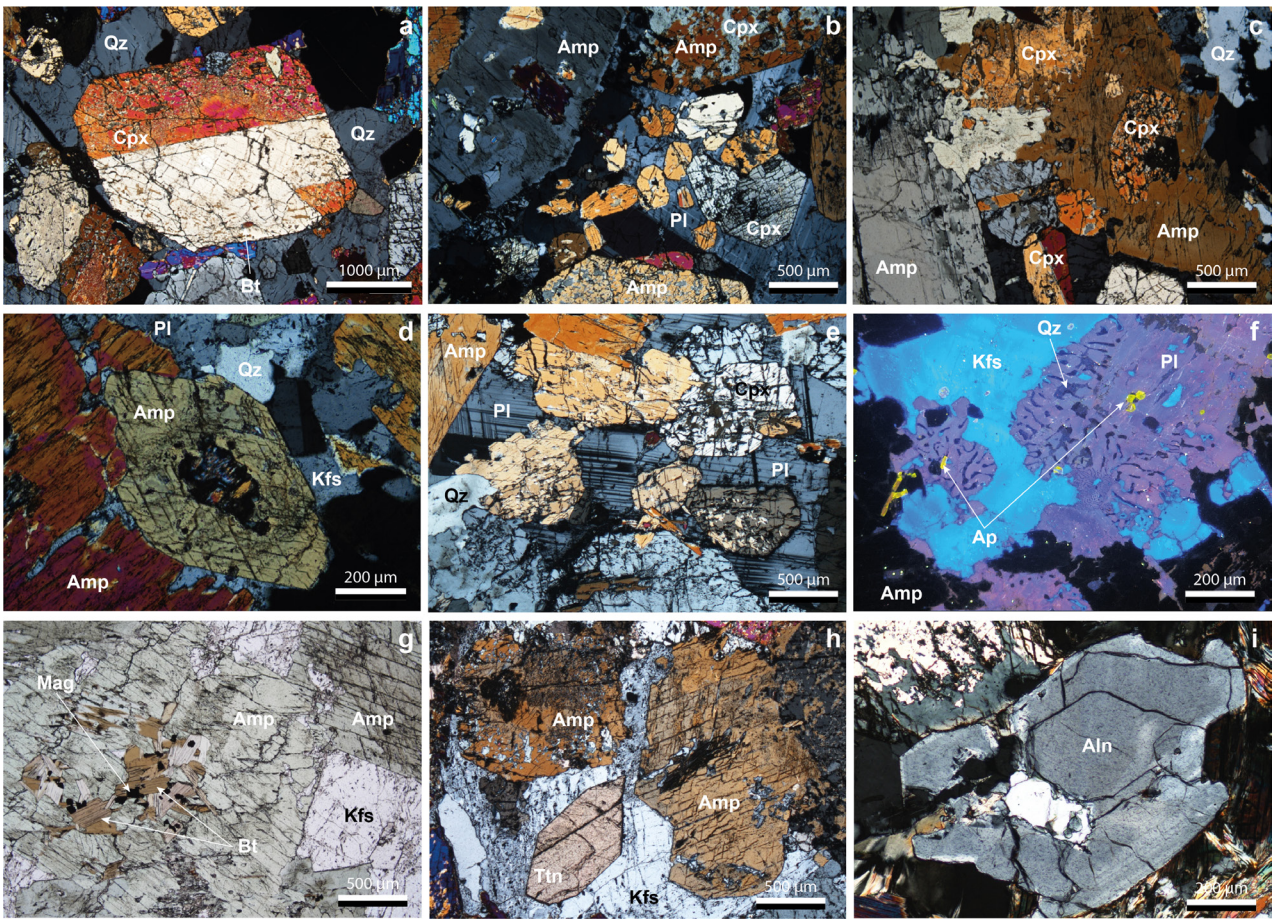

Fig. 3. (figure caption on next page)

Table 3. Representative microprobe analyses of the main mineral phases identified in quartz diorite. Analyses (in wt%) include amphiboles (Amp), clinopyroxene (Cpx), plagioclases (Pl), potassium feldspar (Kfs), biotite (Bt), chlorite (Chl), and epidote (Ep). Amp I_C – Type I amphibole core, Amp I_R – Type I amphibole rim, Amp II – Type II amphibole. Elements in the lower part of the table are calculated values per formula unit, based on the corresponding number of oxygens. An. No. denotes the analysis number.

Sample	C3-1	C4-1	C4-1	C7-3	C4-1	C7-3	C4-1	C7-3	C3-1	C4-1	C7-3	C7-3	C3-1	C1-1
Mineral	Amp I_C	Amp I_C	Amp I_R	Amp I_R	Amp II	Amp II	Cpx	Cpx	Pl	Pl	Kfs	Bt	Chl	Ep
An. No.	12	5	6	4	4	3	2	2	10	9	6	8	5	10
SiO_2	44.36	44.35	53.12	51.91	51.91	50.69	54.04	54.23	63.13	61.03	64.36	36.36	28.31	36.94
TiO_2	0.99	1.01	0.21	0.30	0.60	0.71	0.24	0.11	0.27	0.00	0.11	2.72	0.05	1.08
Al_2O_3	10.91	12.71	4.78	5.30	6.04	6.50	1.92	1.42	22.84	25.00	18.91	14.14	19.13	21.76
Cr_2O_3	0.06	0.00	0.00	0.00	0.00	0.00	0.00	0.00	0.42	0.00	0.00	0.07	0.00	1.40
FeO	13.69	9.31	6.64	7.13	6.77	7.90	3.38	3.35	0.10	0.11	0.07	21.38	18.66	10.62
MnO	0.50	0.15	0.21	0.17	0.20	0.14	0.12	0.11	0.12	0.02	0.06	0.25	0.39	0.13
MgO	11.63	14.32	18.69	17.97	18.03	17.25	15.36	15.58	0.01	0.00	0.01	11.81	19.61	0.22
CaO	12.21	12.20	12.61	12.67	12.81	12.42	24.05	24.08	4.48	6.25	0.04	0.01	0.09	23.24
Na_2O	1.17	1.80	0.49	0.49	0.56	0.55	0.39	0.32	7.52	7.92	0.88	0.07	0.02	0.01
K_2O	1.25	0.60	0.26	0.29	0.27	0.39	0.00	0.00	0.35	0.36	14.76	9.83	0.03	0.01
BaO	0.00	0.25	0.00	0.04	0.05	0.06	0.01	0.00	0.00	0.03	1.49	0.00	0.00	0.00
Total	96.77	96.70	97.01	96.27	97.23	96.62	99.49	99.18	99.22	100.73	100.67	96.63	86.29	95.41
Oxygens	23	23	23	23	23	23	6	6	8	8	8	22	28	12.5
Si	6.56	6.39	7.48	7.39	7.31	7.23	1.98	1.99	2.81	2.70	2.98	5.56	2.29	3.08
Ti	0.11	0.11	0.02	0.03	0.06	0.08	0.01	0.00	0.01	0.00	0.00	0.32	0.00	0.07
Al	1.90	2.16	0.79	0.89	1.00	1.09	0.08	0.06	1.20	1.30	1.03	2.54	1.83	2.14
Cr	0.01	0.00	0.00	0.00	0.00	0.00	0.00	0.00	0.01	0.00	0.00	0.00	0.00	0.09
Fe^{3+}	0.51	0.55	0.18	0.21	0.21	0.23	0.00	0.00	0.00	0.00	0.00	0.00	0.00	0.00
Fe^{2+}	1.18	0.58	0.63	0.64	0.61	0.72	0.10	0.10	0.00	0.00	0.00	2.74	1.26	0.74
Mn	0.06	0.02	0.03	0.02	0.02	0.02	0.00	0.00	0.00	0.00	0.00	0.04	0.03	0.01
Mg	2.56	3.07	3.92	3.82	3.79	3.67	0.84	0.85	0.00	0.00	0.00	2.70	2.37	0.03
Ca	1.93	1.88	1.90	1.93	1.93	1.90	0.94	0.95	0.21	0.30	0.00	0.00	0.01	2.08
Na	0.34	0.50	0.13	0.14	0.15	0.15	0.03	0.02	0.65	0.68	0.08	0.02	0.00	0.00
K	0.24	0.11	0.05	0.05	0.05	0.07	0.00	0.00	0.02	0.02	0.87	1.92	0.00	0.00
Ba							0.00	0.00	0.00	0.00	0.00	0.00	0.00	0.00
Total	15.41	15.38	15.14	15.12	15.15	15.15	3.99	3.99	4.91	5.00	4.97	15.82	7.79	8.24

Petrography and mineral chemistry

Under the optical microscope, the rock exhibits a heterogeneous texture. Clinopyroxene is the dominant mineral, accounting for approximately 35–40% of the rock (Fig. 3). The average grain size of clinopyroxene is 3.4 mm, with the largest crystals reaching 7.6 mm. Amphiboles are the second most abundant mineral phase, comprising up to 30% of the sample. Plagioclases makes up 10–15% of the rock, with an average grain size of 1.63 mm and maximum grains reaching 5.6 mm. Potassium feldspar (i.e., orthoclase) represents about 10% of the quartz diorite; its average grain size is 1.57 mm, with the largest grains measuring up to 5.2 mm.

Minor mineral phases include quartz, biotite, titanite, apatite, magnetite, and epidote group minerals (allanite) with average grain sizes ranging from 0.08 mm (apatite) to 1.1 mm (quartz). Together, these minerals account for 10–15% of the sample. Secondary minerals identified include chlorite, and calcite.

The remaining microscopic and microchemical characteristics are described below for individual minerals. Representative mineral analyses are presented in Table 3.

Fig. 3. Microphotographs of quartz diorite. (a) An idiomorphic, twinned clinopyroxene grain surrounded by smaller clinopyroxene and anhedral quartz grains. Sample C7-3. (b) Amphibole replaces clinopyroxene in an irregular patchy pattern (upper right). Clinopyroxene grains form small clusters enclosed in plagioclase, producing a poikilitic texture. Sample C7-3. (c) Amphibole replacing clinopyroxene completely envelops the grain, producing an uralitic texture. Sample C7-3. (d) An idiomorphic amphibole grain is surrounded by quartz, plagioclase and orthoclase grains. Sample C6-2. (e) Clinopyroxene, quartz and biotite grains enclosed in plagioclase with polysynthetic twins forming a poikilitic texture. Amphibole is visible in the upper-left corner. Sample C8-3. (f) Potassium feldspar (orthoclase) replacing plagioclase forms a myrmekitic texture at their contact. Small apatite inclusions in plagioclase are clearly visible. Sample C3-1. (g) Inclusions of biotite and magnetite occur within amphibole. Sample C5-2. (h) Idiomorphic titanite and amphibole grains surrounded by orthoclase. Sample C10-1. (i) A large allanite grain. Sample C8-3. Abbreviations: Aln–Allanite, Amp–amphiboles, Bt–biotite, Cpx–clinopyroxene, Kfs–potassium feldspar (orthoclase), Mag–magnetite, Pl–plagioclases, Qz–quartz, Ttn–titanite. Crossed polars (a–e, h, i); parallel polars (g); cathodoluminescence (f).

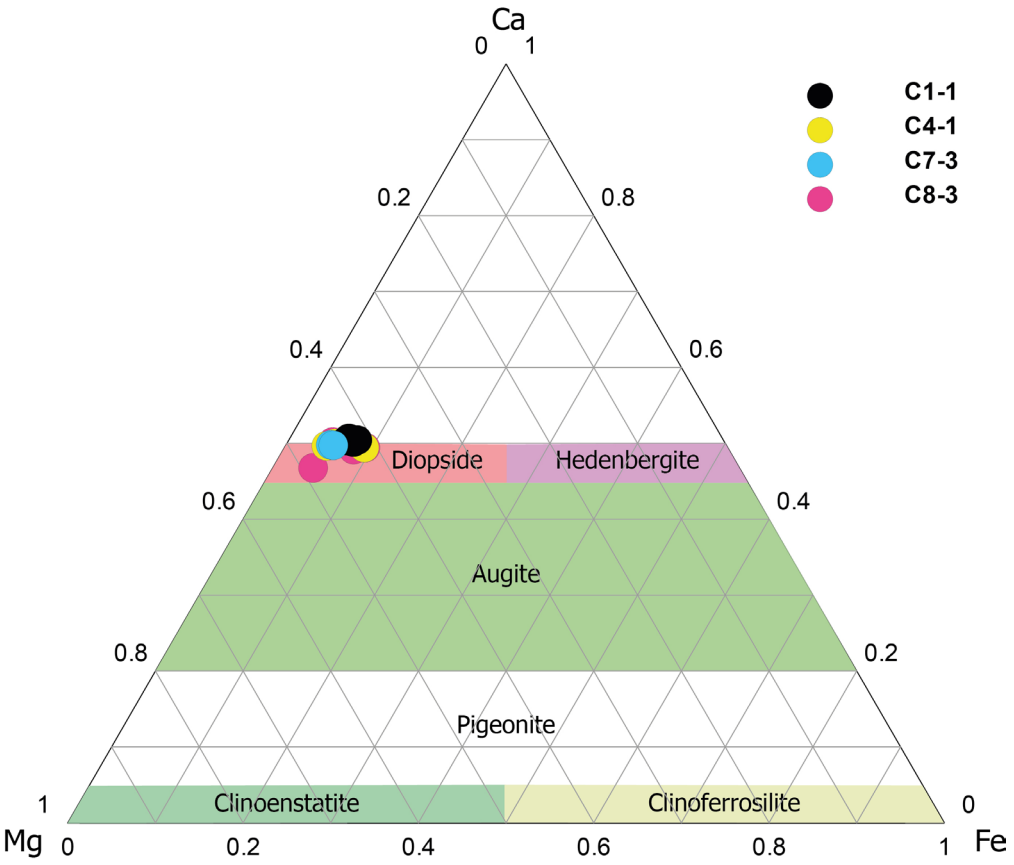

Fig. 4. Classification of clinopyroxene grains in a triangular diagram, following Poldervaart & Hess (1951).

Clinopyroxene

They occur in hypidiomorphic to idiomorphic forms. They often occur as simple twins (Fig. 3a). In some places, idiomorphic pyroxene grains are clustered in one area (Fig. 3b). They are often overgrown by amphiboles (Fig. 3c), which is a result of the uralitization process. They correspond in composition to diopside (Fig. 4) and have values of X_{Ca} = 0.47–0.51, X_{Mg} = 0.41–0.49, and X_{Fe} = 0.05–0.09.

Amphiboles

Two types of amphiboles can be distinguished. Type I amphibole occurs as xenomorphic individual grains (Fig. 5a) and only rarely form hypidiomorphic (Fig. 5b) to idiomorphic shapes (Fig. 3d). Their average size is approximately 4.15 mm. In Type I amphibole core and rim parts have slightly different composition (Fig. 5c). The average core/rim compositions are as follows: X_{Ca} = 0.31/0.30, X_{Mg} = 0.44/0.56, X_{Fe} = 0.25/0.14, and Ti = 0.11/0.03 atoms per formula unit (apfu). Biotite inclusions are very common in Type I amphibole. Type II amphibole replaces clinopyroxene grains (Figs. 3d and 5b), sometimes forming uralitic texture (Fig. 3e). Their average composition corresponds to X_{Ca} = 0.30, X_{Mg} = 0.55, X_{Fe} = 0.15, and Ti = 0.06 apfu.

According to the nomenclature of Leake et al. (1997) all amphiboles are calcic (^{B}Ca>1.5 apfu; with an average Ca content of 1.9 apfu). Type I amphibole cores are classified as magnesiohornblende, tschermakite, edenite, pargasite, or magnesiohastingsite. Type I amphibole rims are classified as magnesiohornblende and actinolite. All Type II amphibole grains belong to magnesiohornblende (Fig. 6).

Based on their Al content, amphiboles can be grouped into two distinct clusters, as shown in the graphs in Figure 7. Amphiboles with higher Al content correspond to Type I amphibole cores, while those with lower Al content belong to Type I amphibole rims and Type II amphibole grains. A positive correlation of Al in T sites with ^{A}(Na + K) for both groups indicates the importance of the edenite exchange (Fig. 7a). Only a slight positive correlation between ^{IV}Al and ^{C}Ti indicates that the Ti-Tschermak exchange substitution is not significant (Fig. 7b). Calcium at the B site shows a slightly positive correlation in the Type I amphibole rims and Type II amphibole grains and a slightly negative one in the Type I amphibole cores; however, the plagioclase exchange is insignificant in both cases (Fig. 7c). The Al-Tschermak substitution is reflected in

the relationship between ^{VI}Al and ^{IV}Al and shows a good positive correlation in the Type I amphibole rims and Type II amphibole grains. In the Type I amphibole cores, however, no correlation is observed (Fig. 7d).

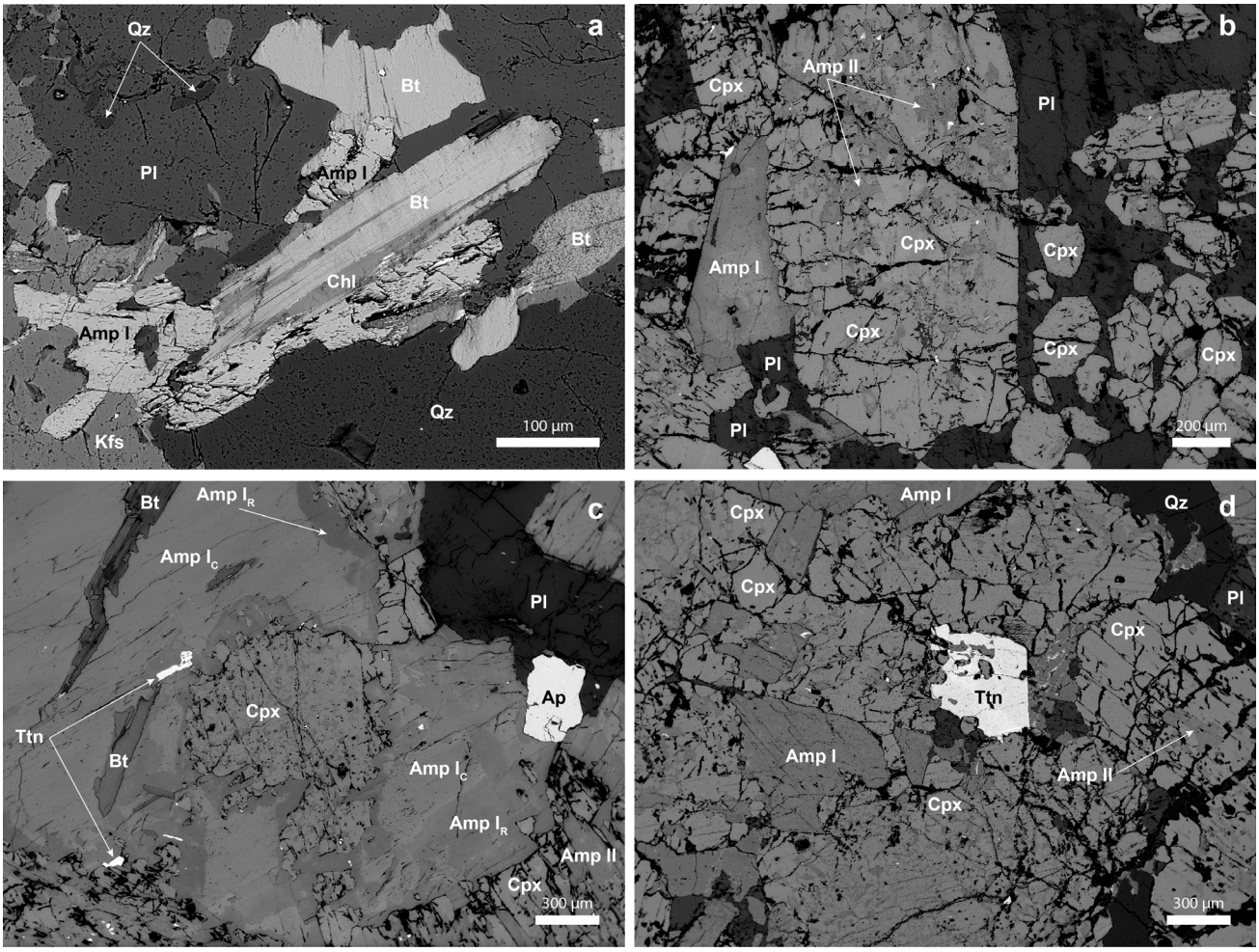

Fig. 5. Backscattered electron images of quartz diorite. (a) Type I amphibole grains are often heavily replaced. Together with plagioclase, quartz, and potassium feldspar (orthoclase), they form a paragenesis suitable for Al-in-amphibole barometry. Biotite grain in the centre is partly chloritized (darker parts). Sample C7-3. (b) A large clinopyroxene grain is partly replaced by Type II amphibole. Type I amphibole is hypidiomorphic and has different core and rim compositions. A large plagioclase grain is enveloping numerous smaller clinopyroxene grains forming a poikilitic texture. Sample C4-1. (c) Type I amphibole grains with well-distinguished core (pale–IC) and rim (dark–IR) parts, clinopyroxene, plagioclase, small titanite, and an apatite grain next to plagioclase are visible. Sample C8-3. (d) A large titanite inclusion in clinopyroxene, Type I amphibole, and Type II amphibole replacing clinopyroxene grains. Sample C7-3. Abbreviations: Amp–amphiboles, Bt–biotite, Cpx–clinopyroxene, Kfs–potassium feldspar (orthoclase), Pl–plagioclases, Qz–quartz, Ttn–titanite.

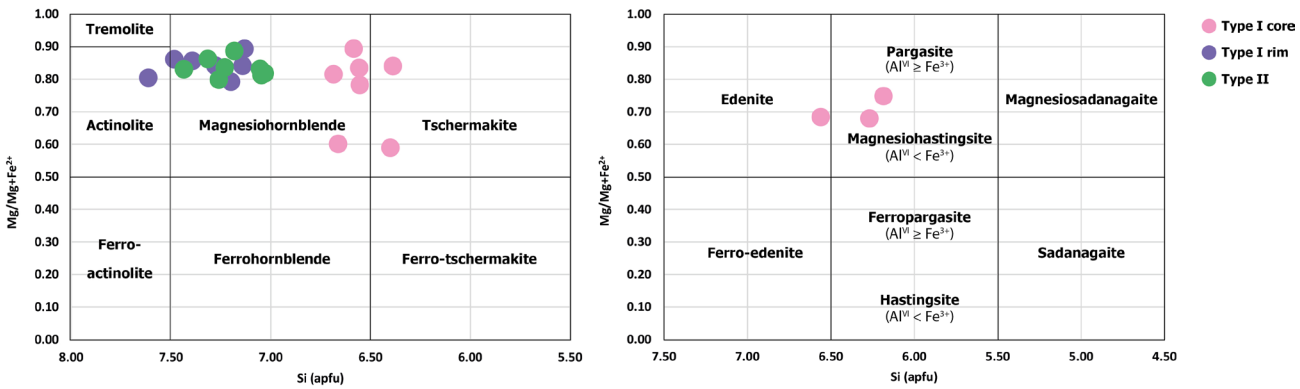

Fig. 6. The composition of Type I and Type II amphibole is shown in the calcic amphibole classification diagram (adapted from Leake et al., 1997).

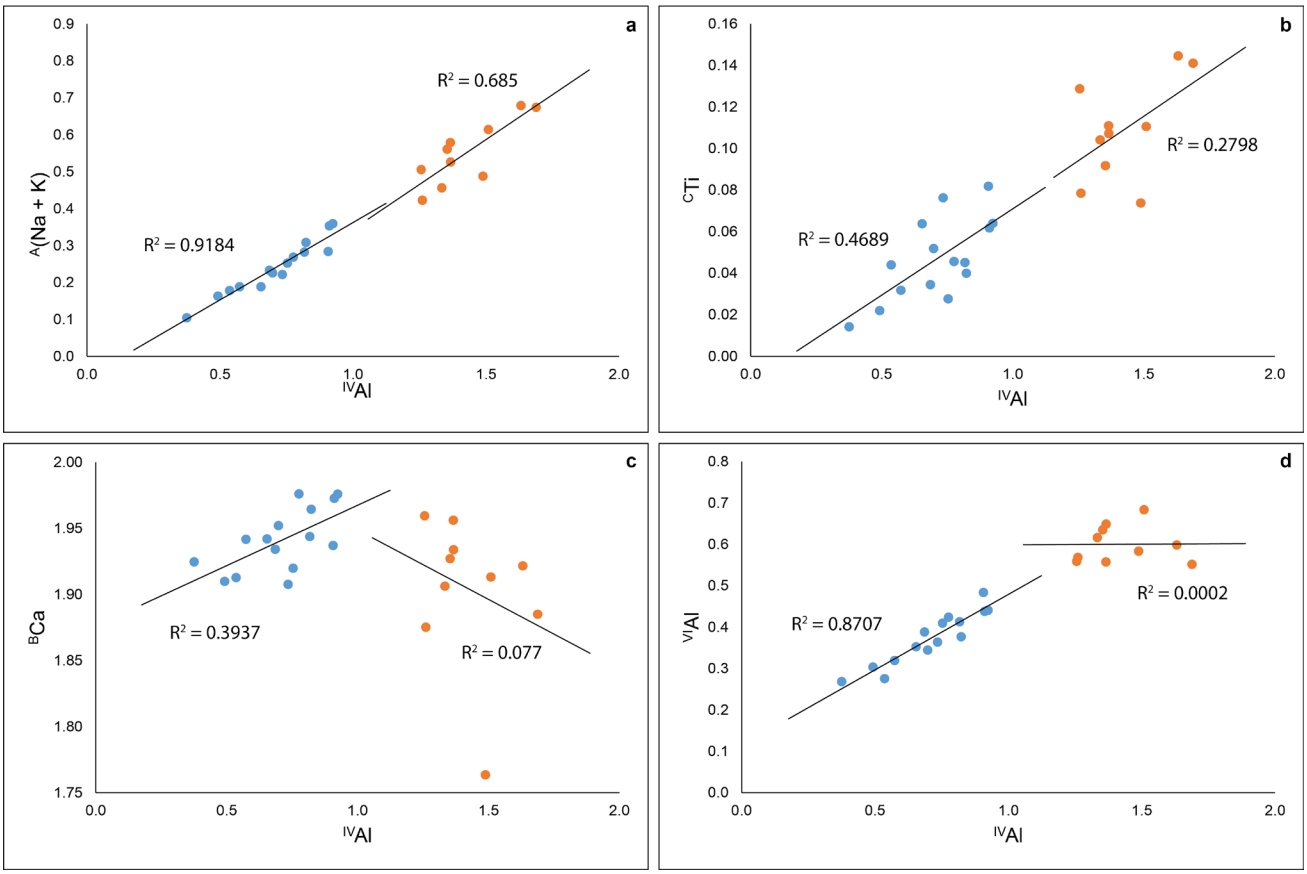

Fig. 7. Site occupancies and exchange mechanisms in amphiboles: (a) edenite exchange, (b) Ti–Tschermak exchange, (c) plagioclase exchange, and (d) Al–Tschermak exchange. Note that scales on the x- and y-axes are not equal.

Feldspars

Plagioclases are usually quite homogeneous; however, in some grains, zoning and polysynthetic twinning (Fig. 3e) can be recognised. Occasionally, a poikilitic texture is present, where grains of other minerals, such as clinopyroxene, quartz, and biotite, are enclosed within larger plagioclase grains (Fig. 3b). A myrmekitic texture at the boundary between plagioclase and orthoclase may also be observed, formed as a result of reaction between these two minerals (Fig. 3f). Plagioclases are intermediate in composition, with X_{Ab} = 0.61–0.73, corresponding to the feldspar series from oligoclase to andesine (Fig. 8), with a low proportion of orthoclase (up to ~2.56 mol%).

Potassium feldspars are represented by orthoclase commonly forming characteristic perthitic structure. It mostly fills the spaces between the femic minerals. In some places, orthoclase grains replace plagioclases (Fig. 3f). The measured composition of potassium feldspar shows 85.43–91.72 mol% orthoclase, 8.12–14.32 mol% albite, and 0.16–0.32 anorthite. Some potassium feldspar grains contain BaO, with an average content of 1.49 wt%.

Minor mineral phases

Quartz occurs in all samples. It typically occurs as small grains, with larger individual crystals observed only occasionally. The average grain size is 1.1 mm, and the largest measured grain is 6 mm. Quartz makes up 5–10% of the total rock. It occurs as small inclusions in minerals but mostly forms xenomorphic grains filling the spaces between larger crystals (Figs. 3a and 5a). **Biotite** is also present among the femic minerals, but in subordinate amounts not exceeding 3%. The average grain size is 0.67 mm, and the largest measured grain is 0.84 mm. It is brown in colour and exhibits strong pleochroism. It occurs in hypidiomorphic grains. Biotite most frequently appears as inclusions in amphiboles (Fig. 3g), or as individual grains (Fig. 5a). It is partly replaced by chlorite (Fig. 5a).

Accessory mineral phases include apatite, titanite, and epidote group minerals. **Titanite** is present as idiomorphic grains (Figs. 3h and 5d). The average grain size is 0.74 mm, and the largest measured grain is 1.4 mm. It usually accounts for 1–2% of the total rock. It often occurs as an inclusion in plagioclases, orthoclase, clinopyroxene, and amphiboles (Fig. 5c). **Apatite** occurs as small

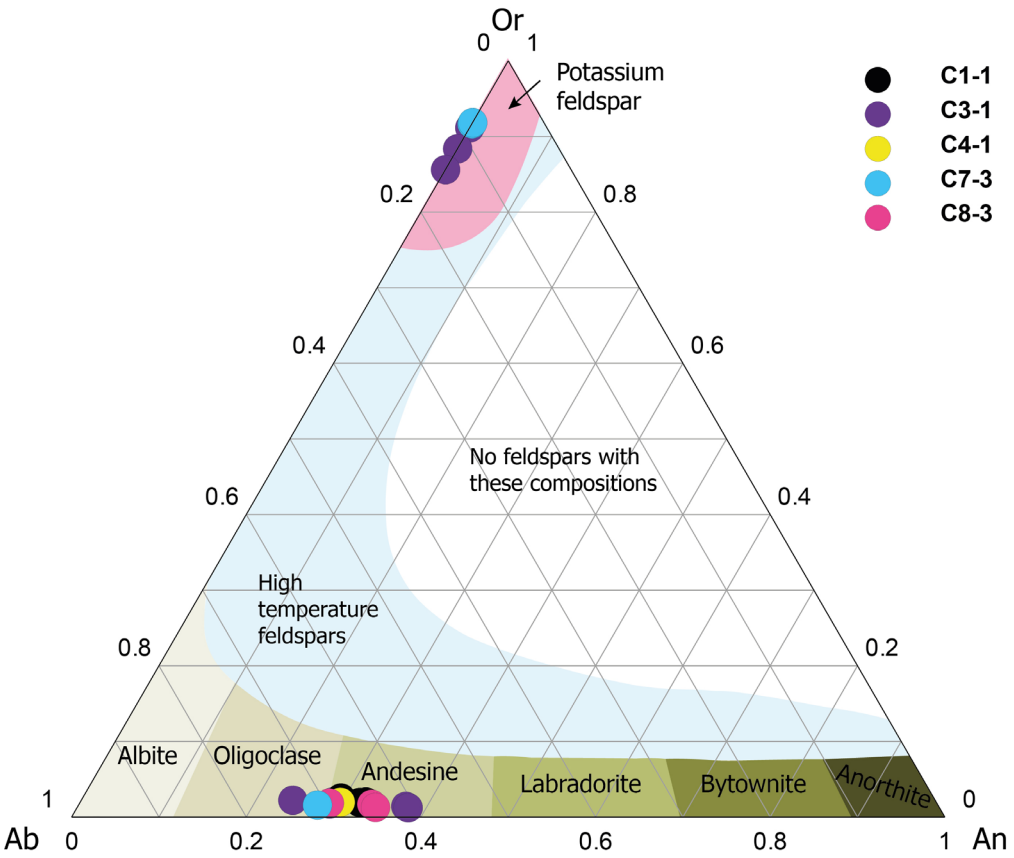

Fig. 8. Composition of feldspars shown in the classification diagram of orthoclase (Or), albite (Ab), and anorthite (An) (adapted from Deer et al., 2001).

grains; the average grain size is 0.08 mm, while the largest measured grain is 0.13 mm. Apatite grains account for up to 1% of the total rock. They occur as rod-shaped grains, often as inclusions in plagioclases, and orthoclase (Fig. 3f). **Epidote group minerals** (most probably allanite) are very rare and enriched in REEs (Fig. 3i). **Magnetite** occurs as small grains included in amphiboles, often accompanied by biotite (Fig. 3g).

Secondary minerals are abundant in more intensely differentiated and/ or metasomatically altered samples and are mainly **chlorite** replacing biotite and amphibole grains (Fig. 5a) and **calcite** replacing clinopyroxene and feldspar grains.

Geothermobarometry

Data selection and validation for geothermobarometric calculations

Nimis (1995) developed a crystal-structure–based clinopyroxene barometer. This calibration is restricted to C2/c clinopyroxene crystallized from basaltic melts. Because the alumina content of the parental magma strongly influences clinopyroxene chemistry, it is not applicable to high-alumina magmas. Later revision by Nimis and Ulmer (1998) produced a new calibration valid only for clinopyroxene that satisfy the following conditions: (Ca + Na) > 0.5 apfu, $Mg/(Mg + Fe^{2+}) > 0.7$, and Al_2O_3/SiO_2 (wt%) < 0.375 (i.e., Al2O3 < 18 wt%).

All investigated clinopyroxene grains are classified as diopside, which belongs to the C2/c space group, therefore meeting the crystal-structure criterion. Furthermore, all the measured clinopyroxene grains satisfy the chemical restrictions. (Ca + Na) contents vary between 0.9 and 1.0, $Mg/(Mg + Fe^{2+})$ values are 0.8–0.9 and Al_2O_3/SiO_2 ranges from 0.012 to 0.039. Therefore, we find all the measurements to meet the requirements for applying geothermobarometric calculations.

The amphibole composition varies not only with pressure, temperature and coexisting mineral assemblage, but also with oxygen fugacity (fO_2) in melt, which controls the Fe# and Fe^{3+}/Fe_{TOT} ratios. Spear (1981) and Anderson & Smith (1995) classify Fe# values in the range from 0 to 0.6 as high, between 0.6 and 0.8 as medium, and 0.8 to 1 as low oxygen fugacity. Low fO_2 favours the insertion of Fe^{2+} in the amphibole lattice, which promotes the substitution of Mg by Al during the Tschermak exchange. A low oxygen fugacity therefore leads to high contents of aluminium in amphibole. Therefore, Anderson & Smith (1995) recommends using only amphiboles with Fe# ≤ 0.65. On the other hand, a high fO_2 leads to a preferred incorporation of Fe^{3+} into the lattice, which

preferably substitutes Al, thus keeping the content of aluminium in amphibole low. Anderson & Smith (1995) recommend using amphiboles with Fe^{3+}/Fe_{TOT} ratio ≥ 0.25, while Schmidt (1992) sets this ratio at ≥ 0.2. Presence of accessory minerals can, according to Ishihara (1977), suggest conditions of oxygen fugacity. Magnetite and titanite in igneous rocks point to a high oxygen fugacity, while ilmenite indicates a low oxygen fugacity. In general, amphibole crystallizing under high fO_2 gives better and more reliable geothermobarometry results than those growing under low fO_2 as experimental calibrations were carried out under medium to high oxygen fugacity (Stein & Dietl, 2001).

Measured amphibole grains in our case show different ratios of Fe^{3+}/Fe_{TOT} and Fe#, which can be seen in Figure 9. All grains have Fe# well below 0.65, which according to Spear (1981) and Anderson & Smith (1995) indicates high oxygen fugacity. Fe^{3+}/Fe_{TOT} ratio of all grains are within the recommended values apart from grains Amp6 (sample C8-3, analysis no. 10) and Amp8 (sample C8-3, analysis no. 16). Therefore, these measurements are excluded from further calculations. However, it is important to stress that the Fe^{3+} content is based on stoichiometric calculations and not on direct measurements of the amount of Fe^{3+} and Fe^{2+} in amphiboles. In addition, magnetite and titanite were found as accessory minerals, which point to high fO_2 as well, suggesting the overall suitability of the measured amphibole samples for geothermobarometry.

The empirical biotite thermometer equation of Henry et al. (2005) is strictly valid only for X_{Mg} = Mg/(Mg + Fe) = 0.275–1.000 and Ti = 0.04–0.60 apfu calculated on the basis of 22 oxygen atoms, with temperatures in the range 480–800 °C. All our measured biotite grains meet the required criteria (X_{Mg} = 0.496–0.799 and Ti = 0.16–0.34 apfu, so we were able to apply the thermometer.

Clinopyroxene thermobarometry

Results of thermobarometric calculations of clinopyroxene are presented in Table 4, where pressures and temperatures of all considered samples are shown, as well as averages and standard deviations of individual thermobarometers. Calculated crystallization temperatures using the pressure-uncorrected thermometers of Dal Negro et al. (1982) and Molin & Zanazzi (1991) yielded values of approximately 900 °C. Pressure-dependent thermometer of Bertrand & Mercier (1985), calculated at 7 kbar results in lower temperatures, averaging around 842 °C, though with standard deviation of 61 °C.

Pressures of crystallization based on barometer of Nimis (1999) result in an average of 7.73 kbar. Temperature corrected barometer of Nimis & Ulmer (1998) at 900 °C on average shows 6.73 kbar. Standard deviations in calculated pressures are 0.94 and 0.79 kbar for Nimis (1999) and Nimis & Ulmer (1998), respectively. Positions of thermobarometers calculated for the representative clinopyroxene grain Cpx9 (sample C4-1, analysis no. 5) in the P–T diagram are shown in Figure 10.

Amphibole thermobarometry

Results of thermobarometric calculations using the above-listed thermometers and barometers applied to selected amphiboles are summarized in Table 4. Type I amphibole cores crystallized at av-

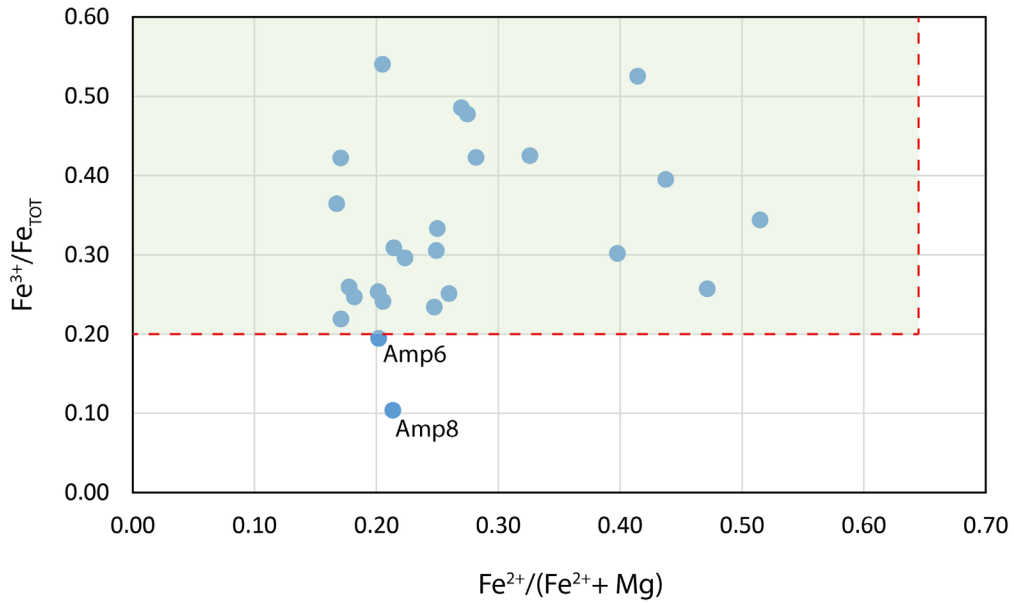

Fig. 9. Ratios of Fe^{2+}/Fe_{TOT} plotted against Fe# [$Fe^{2+}/(Fe^{2+}$ + Mg)] for analysed amphiboles. Amp6 (sample C8-3, analysis no. 10) and Amp8 (sample C8-3, analysis no. 16) fall outside the recommended values, so we excluded them from further calculations.

Table 4. Temperatures T(°C) and pressures P(kbar) calculated for selected clinopyroxene, amphibole and biotite grains. The applied geothermobarometers are listed in Table 2, along with their corresponding abbreviations. The assumed pressure for the calculation of temperatures with the BM85 thermometer was 7.0 kbar. The assumed temperature for the calculation of pressures with the NU98 barometer was 900 °C.

Grain	An. No.	Sample	T(DN82)	T(BM85)	T(MZ91)	P(NU98)	P(N99)
Clinopyroxene							
Cpx2	8	C8-3	907	750	906	6.75	7.05
Cpx3	3	C8-3	897	835	904	6.54	7.21
Cpx4	5	C8-3	901	854	905	5.51	6.82
Cpx6	18	C8-3	897	883	904	5.86	7.33
Cpx7	10	C7-3	899	918	904	7.38	8.43
Cpx8	11	C7-3	907	848	906	6.42	7.86
Cpx9	5	C4-1	903	930	906	8.27	9.18
Cpx10	4	C1-1	901	818	905	8.07	8.63
Cpx12	12	C1-1	909	746	907	5.76	7.04
Average			902	842	905	6.73	7.73
Standard deviation			4	61	1	0.94	0.79

			T(O84)	T(BH90)	T(HB94)	P(S92)	P(AS95)	Grain	An. No.	Sample	T(L84)	T(H05)
Type I amphibole core								Biotite				
Amp2	3	C8-3	669	673	634	6.16	6.23	Bt1	11	C8-3	697	698
Amp 4	5	C8-3	654	674	671	6.33	6.56	Bt2	12	C8-3	674	673
Amp10	18	C8-3	672	673	659	6.47	6.50	Bt3	8	C7-3	638	677
Amp13	10	C7-3	632	695	804	6.69	7.12	Bt4	9	C7-3	658	694
Amp14	11	C7-3	638	668	773	5.60	5.93	Bt5	12	C7-3	651	685
Amp17	5	C4-1	676	688	842	7.26	7.25	Bt6	13	C7-3	695	697
Amp20	4	C1-1	699	664	803	5.56	5.25					
Amp22	3	C3-1	711	719	775	7.44	6.86					
Amp23	12	C3-1	677	678	654	6.04	6.02					
Amp24	13	C3-1	716	705	709	7.44	6.76					
Average			675	684	732	6.50	6.45				669	687
Standard deviation			28	18	75	0.70	0.61				24	11
Type I amphibole rim												
Amp3	4	C8-3	586	605	587	2.08	2.18					
Amp5	7	C8-3	599	624	707	2.81	3.03					
Amp9	17	C8-3	578	615	587	2.49	2.60					
Amp12	4	C7-3	583	591	664	1.22	1.20					
Amp18	6	C4-1	571	575	596	0.77	0.61					
Amp21	11	C1-1	593	624	696	2.67	2.87					
Average			585	606	640	2.01	2.08					
Standard deviation			10	20	56	0.83	0.97					
Type II amphibole												
Amp1	2	C8-3	600	616	575	2.67	2.88					
Amp7	15	C8-3	607	610	691	1.92	2.08					
Amp11	3	C7-3	636	613	649	2.19	2.36					
Amp15	3	C4-1	643	629	730	3.57	3.78					
Amp16	4	C4-1	621	601	688	1.76	1.92					
Amp25	16	C1-1	622	634	758	3.45	3.72					
Average			622	617	682	2.59	2.79					
Standard deviation			17	12	64	0.77	0.81					

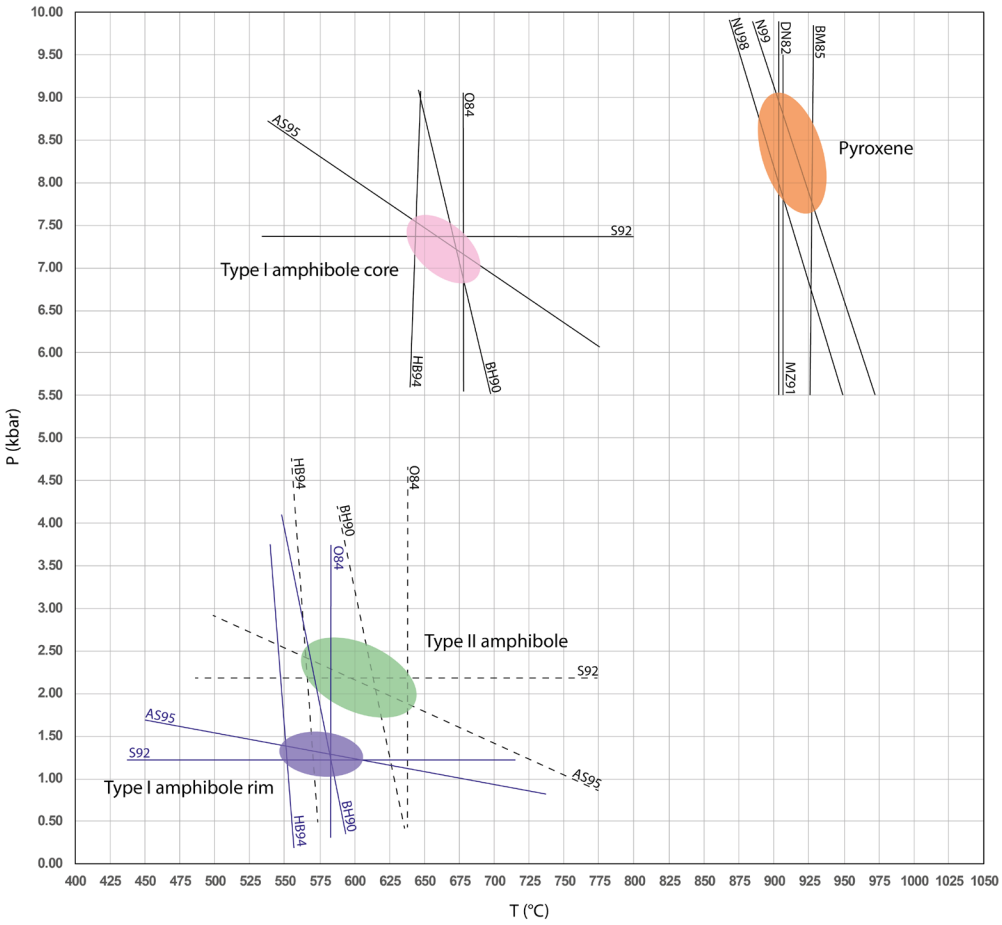

Fig. 10. Positions of thermobarometers for representative clinopyroxene grain Cpx9 (sample C4-1, analysis no. 5), Type I amphibole core – Amp23 (sample C3-1, analysis no. 12), Type I amphibole rim – Amp12 (sample C7-3, analysis no. 4), and Type II amphibole replacing clinopyroxene – Amp11 (sample C7-3, analysis no. 3). The applied geothermobarometers are listed in Table 2, along with their corresponding abbreviations.

erage temperatures of 675 °C, 732 °C, and 684 °C calculated by equations of Otten (1984), Holland & Blundy (1994), and Blundy & Holland (1990), respectively. The latter two thermometers are pressure-corrected using pressures derived from Schmidt (1992) and thus considered more reliable. Average pressures at the time of equilibrium are calculated to be 6.50 kbar and 6.45 kbar based on barometers of Schmidt (1992) and temperature-corrected Anderson & Smith (1995), respectively.

Type I amphibole rims show temperatures of 585 °C, 640 °C, and 606 °C based on calibrations of Otten (1984), Holland & Blundy (1994), and Blundy & Holland (1990), respectively. Average pressures from Schmidt (1992) and Anderson & Smith (1995) are estimated at 2.01 kbar and 2.08 kbar, respectively. These amphiboles show high variations in calculated pressures within both barometers used. Standard deviations are 0.83 kbar and 0.97 kbar for Schmidt (1992) and Anderson & Smith (1995), respectively. Consequently, this is also reflected in the pressure-corrected temperatures calculated using Holland & Blundy (1994) and Blundy & Holland (1990).

Type II amphibole grains show average temperatures of 622 °C, 682 °C, and 617 °C, which were determined based on calibrations of Otten (1984), Holland & Blundy (1994), and Blundy & Holland (1990), respectively. Determined average pressures are calculated to be 2.59 kbar and 2.79 kbar with standard deviations of 0.77 kbar and 0.81 kbar using barometers of Schmidt (1992) and Anderson & Smith (1995), respectively.

Thermobarometers applied to representative amphibole grains are shown in Figure 10. The Type I amphibole core is represented by grain Amp23 (sample C3-1, analysis no. 12); the Type I amphibole rim, by grain Amp12 (sample C7-3, analysis no. 4); and the Type II amphibole replacing clinopyroxene, by grain Amp11 (sample C7-3, analysis no. 3). Crystallization conditions of the Type I amphibole cores are clearly distinguishable from those of the Type I amphibole rims and Type II amphibole grains. On the other hand, pressures and temperatures of the latter two groups are very similar and fall close to the estimated errors of pressure determination, making them indistinguishable based on calculations alone.

Biotite thermometry

The analysed biotite grains yielded average temperatures of 669 °C and 687 °C according to the thermometers of Luhr et al. (1984) and Henry et al. (2005), respectively. The calculated temperatures are shown in Table 4. The measured biotite grains were petrographically associated with Type I amphibole cores. They were in contact with amphiboles or completely enclosed within Type I amphibole in the core regions (Fig. 5a, c).

Discussion

Quartz diorite body is part of the larger PIC; therefore, we should consider its crystallization in the light of the PIC formation. Poli et al. (2020) explain its formation as a series of chemically diverse melt pulses intruding different crust levels, leading to a variety of observed lithologies. Quartz diorite is considered the first to form from basaltic melts by cumulus processes. Modelling of the cumulus process of quartz diorite has shown that the most important cumulus mineral was clinopyroxene, whereas amphiboles plus plagioclases were subordinate (Poli et al., 2020). Our thermobarometric calculations show that the clinopyroxene formed first, at the highest pressures and temperatures ranging from 840–900 °C and 6.70–7.70 kbar. This is consistent with modelled cumulus process as well as with petrographic observations, which indicate that amphiboles crystallized later, replacing the early-formed pyroxene and sometimes forming uralitic texture.

The first amphiboles to crystallize were Type I amphibole cores. They crystallized at 670–730 °C and 6.45–6.50 kbar. These conditions are consistent with calculations of amphiboles crystallization in the less evolved GDT. Poli et al. (2020) determined average temperatures of 666 °C and pressures of 6.08 kbar. Similar averages of 695 °C and 6.91 kbar were obtained by Sotelšek (2019). These similarities in pressures and temperatures of amphiboles from quartz diorite and the less evolved GDT suggest their coeval formation. Temperatures derived from biotite grains and Type I amphibole cores are consistent, confirming the accuracy of the calculations and supporting the interpretation that these amphiboles crystallized contemporaneously with the less evolved GDT.

Type I amphibole rims were formed at lower P–T conditions near 585–640 °C and ~2.00 kbar. Slightly higher conditions of 617–682 °C and 2.59–2.79 kbar were calculated from Type II amphibole grains. The distinctly different chemical composition of the Type I amphibole rims and the replacement and assimilation of pyroxene by Type II amphibole grains compared to Type I amphibole cores clearly point to their later formation. These results can be related to the emplacement of the shallower parts of the GDT pluton (more evolved granodiorite sensu Poli et al., 2020). Sotelšek (2019) reports pressures from the shallower NW parts of the pluton in the range of 2–3 kbar and temperatures of 635–699 °C, which is comparable to the Type I amphibole rims and Type II amphibole growth conditions. Therefore, amphiboles from these two groups are assumed to have formed contemporaneously with the emplacement of more evolved GDT.

Conclusions

Based on the presented data, we can relate all observations and calculations to the evolution of the whole PIC. Quartz diorite body formed in several stages recorded in the pressures and temperatures of formation of clinopyroxene, amphiboles, and biotite. Pyroxene grains were the first to form by cumulus processes at 840–905 °C and 6.70–7.70 kbar, followed by Type I amphibole cores at 675–730°C and 6.45–6.50 kbar, which corresponds to the formation conditions of the less evolved GDT. Coeval with the formation of the more evolved GDT was the formation of Type I amphibole rims and Type II amphibole at 585–640 °C and ~2.00 kbar and 615–680 °C and 2.59–2.79 kbar, respectively. Biotite records similar temperatures of 670–690 °C.

Acknowledgements

The authors acknowledge the financial support of the Slovenian Research and Innovation Agency (ARIS): Research Core Funding No. P1-0195, Young Researchers Program No. 55758, and UNESCO IGCP 637 (Heritage Stone Designation).

References

Altherr, R., Lugović, B., Meyer, H.P. & Majer, V. 1995: Early Miocene postcollisional calc-alkaline magmatism along the easternmost segment of the Periadriatic fault system (Slovenia and Croatia). Mineralogy and Petrology, 54: 225–247. https://doi.org/10.1007/bf01162863

Anderson, J.L. & Smith, D.R. 1995: The Effects of Temperature and f_{O2} on the Al-in-Hornblende Barometer. American Mineralogist, 80/5–6: 549–559. https://doi.org/10.2138/AM-1995-5-614

ARSO, 2018: Varstvo naravnih vrednot. Ljubljana: Agencija Republike Slovenije za okolje. Inter-

net: https://zrsvn-varstvonarave.si/kaj-varujemo/naravne-vrednote/ (18. 9. 2018).

Benesch, F. 1917: Beiträge zur Gesteinskunde des östlichen Bachergebirges (Südsteiermark). Mitteilungen des Alpenländischen Geologischen Vereines, 10: 161–183.

Bertrand, P. & Mercier, J.-C.C. 1985: The mutual solubility of coexisting ortho- and clinopyroxene: toward an absolute geothermometer for the natural system? Earth and Planetary Science Letters, 76/1–2: 109–122. https://doi.org/10.1016/0012-821X(85)90152-9

Blundy, J.D. & Holland, T.J.B. 1990: Calcic amphibole equilibria and a new amphibole-plagioclase geothermometer. Contributions to Mineralolgy and Petrology, 104: 208–224. https://doi.org/10.1007/BF00306444

Činč, B. 1992: Mineraloške in geokemične značilnosti aplitnih in pegmatitnih žil v pohorskem tonalitu in čizlakitu. Magistrsko delo. Univerza v Ljubljani, Fakulteta za naravoslovje in tehnologijo, Ljubljana: 106 p.

Dal Negro, A., Carbonin, S., Molin, G.M., Cundari, A. & Piccirillo, E.M. 1982: Intracrystalline cation distribution in natural clinopyroxenes of tholeiitic, transitional, and alkaline basaltic rocks. In: Saxena, S.K. (ed.): Advances in Pyhsical Geochemistry, 2: 117–150.

Deer, W.A., Howie, R.A. & Zussman, J. 2001: Rock-forming minerals. 4A, framework silicates, feldspars, 2. ed. Geological Society, London: 972 p.

Dolar-Mantuani, L. 1935: Razmerje med tonaliti in apliti pohorskega masiva. Geološki Anali Balkanskog Poluostrva, 12: 1–165.

Dolar-Mantuani, L. 1940: Diferencijacija magmatskih kamnin na Pohorju. Ljubljana. Razprave matematično-prirodoslovnega razreda: 1–13.

Dolenec, T. 1994: Novi izotopski in radiometrični podatki pohorskih magmatskih kamnin. Rudarsko-metalurški zbornik, 41/3–4: 147–152.

Dolenec, T., Pezdič, J. & Strmole, D. 1987: Isotopic composition of oxygen in igneous rocks of Pohorje = Izotopska sestava kisika v pohorskem tonalitu in čizlakitu). Geologija, 30/1: 231–244.

Droop, G.T.R. 1987: A general equation for estimating Fe^{3+} concentrations in ferromagnesian silicates and oxides from microprobe analyses, using stoichiometric criteria. Mineralogical Magazine, 51: 431–435.

Faninger, E. 1965: Čizlakit v novejši petrografski klasifikaciji. Geologija, 8/1: 263–278.

Faninger, E. 1973: Pohorske magmatske kamenine. Geologija, 16/1: 271–315.

Fodor, L., Balogh, K., Dunkl, I., Pécskay, Z., Korokanai, B., Trajanova, M., Vrabec, M., Vrabec, M., Horváth, P., Janák, M., Lupták, B., Frisch, W., Jelen, B. & Rifelj, H. 2003: Structural evolution and exhumation of the Pohorje-Kozjak Mts., Slovenia. Annales Universitatis Scientiarum Budapestinensis. Sectio Geologica, Tom. 35: 118–119.

Fodor, L.I., Gerdes, A., Dunkl, I., Koroknai, B., Pécskay, Z., Trajanova, M., Horváth, P., Vrabec, M., Jelen, B., Balogh, K. & Frisch, W. 2008: Miocene emplacement and rapid cooling of the Pohorje pluton at the Alpine-Pannonian-Dinaridic junction, Slovenia. Swiss Journal of Geosciences, 101: 255–271. https://doi.org/10.1007/978-3-7643-9950-4_15.

Hammarstrom, J.M. & Zen, E. 1986: Aluminum in hornblende: An empirical igneous geobarometer. American Mineralogist, 71/11-12: 1297–1313.

Helz, R.T. 1982: Chapter 2, Experimental studies of amphibole stability; Phase relations and compositions of amphiboles produced in studies of the melting behavior of rocks. Reviews in Mineralogy & Geochemistry, 9B:279–346. https://pubs.geoscienceworld.org/msa/rimg/article/9B/1/279/87635/Chapter-2-Experimental-studies-of-amphibole

Henry, D.J., Guidotti, C.V. & Thomson, J.A. 2005: The Ti–saturation surface for low–to–medium pressure metapelitic biotites: Implications for geothermometry and Ti–substitution mechanisms. American Mineralogist, 90/2–3: 316–328. https://doi.org/10.2138/am.2005.1498

Hinterlechner-Ravnik, A. 1971. Pohorske metamorfne kamnine = The metamorphic rocks of Pohorje. Geologija, 14/1: 187–226.

Hinterlechner-Ravnik, A. 1973: Pohorske metamorfne kamnine II = The metamorphic rocks of Pohorje mountains II. Geologija, 16/1: 245–270.

Hinterlechner-Ravnik, A. & Moine, B. 1977: Geochemical Characteristics of the Metamorphic Rocks of the Pohorje Mountains. Geologija, 20/1: 107–140.

Hinterlechner-Ravnik, A., Sassi, F.P. & Visona, D. 1991a: The Austridic eclogites, metabasites and metaultrabasites from the Pohorje area (Eastern Alps, Yugoslavia): 1. The eclogites and related rocks. Rendiconti Fisiche Accademia Lincei, 2: 157–173.

Hinterlechner-Ravnik, A., Sassi, F.P. & Visona, D. 1991b: The Austridic eclogites, metabasites and metaultrabasites from the Pohorje area

(Eastern Alps, Yugoslavia): 2. The metabasites and metaultrabasites, and concluding considerations. Rendiconti Fisiche Accademia Lincei, 2: 175–190.

Holland, T. & Blundy, J. 1994. Non-ideal interactions in calcic amphiboles and their bearing on amphibole-plagioclase thermometry. Contributions to Mineralogy and Petrology, 116: 433–447. https://doi.org/10.1007/BF00310910

Ishihara, S. 1977: The magnetite series and ilmenite series granitic rocks. Mining Geology, 27: 293–305. https://doi.org/10.11456/SHIGENCHISHITSU1951.27.293

Janák, M., Froitzheim, N., Lupták, B., Vrabec, M. & Krogh Ravna, E.J. 2004: First evidence for ultrahigh – pressure metamorphism of eclogites in Pohorje, Slovenia: Tracing deep continental subduction in the Eastern Alps. Tectonics, 23: TC5014. https://doi.org/10.1029/2004TC001641

Janák, M., Froitzheim, N., Yoshida, K., Sasinková, V., Nosko, M., Kobayashi, T., Hirajima, T. & Vrabec, M. 2015: Diamond in metasedimentary crustal rocks from Pohorje, Eastern Alps: A window to deep continental subduction. Journal of Metamorphic Geology, 33: 495–512. https://doi.org/10.1111/jmg.12130

Kirst, F., Sandmann, S., Nagel, T.J., Froitzheim, N. & Janák, M. 2010: Tectonic evolution of the southeastern part of the Pohorje Mountains (Eastern Alps, Slovenia). Geologica Carpathica, 61: 451-461. https://doi.org/10.2478/v10096-010-0027-y

Leake, B., Woolley, A.R., Arps, C.E.S. et al. 1997: Nomenclature of Amphiboles: Report of the Subcommittee on Amphiboles of the International Mineralogical Association Commission on New Minerals and Mineral Names. Mineralogical Magazine, 61: 295–321.

Luhr, J.F., Carmichael, I.S.E. & Varekamp, J.C. 1984: The 1982 eruptions of El chichon volcano, Chiapas, Mexico: mineralogy and petrology of the anhydrite-bearing pumices. Journal of volcanology and geothermal research, 23: 69–108. https://doi.org/10.1016/0377-0273(84)90057-X

Mioč, P. 1978: Osnovna geološka karta SFRJ 1:100 000. Tolmač lista Slovenj Gradec. Zvezni geološki zavod, Beograd: 74 p.

Mioč, P. & Žnidarčič, M. 1977. Osnovna geološka karta SFRJ 1:100 000. List Slovenj Gradec. Zvezni geološki zavod, Beograd.

Mioč, P. & Žnidarčič, M. 1989: Osnovna geološka karta SFRJ 1:100 000. Tolmač lista Maribor in Leibnitz. Zvezni geološki zavod, Beograd: 60 p.

Nikitin, V. 1939: Čizlakit – nova kamnina s Pohorja. Ljubljana. Zbornik Priorodoslovnega Društva, 1: 32–36.

Nikitin, V. & Klemen, R. 1937: Diorit-pirokseniti v okolici Čizlaka na Pohorju. Geološki Anali Balkanskog Poluostrva, 14/2: 149–198.

Nimis, P. 1995: A clinopyroxene geobarometer for basaltic systems based on crystal-structure modeling. Contributions to Mineralogy and Petrolgy, 121: 44–125. https://doi.org/10.1007/s004100050093

Nimis, P. 1999: Clinopyroxene geobarometry of magmatic rocks. Part 2. Structural geobarometers for basic to acid, tholeiitic and mildly alkaline magmatic systems. Contributions to Mineralogy and Petrolgy, 135: 62–74. https://doi.org/10.1007/s004100050498

Nimis, P. & Ulmer, P. 1998: Clinopyroxene geobarometry of magmatic rocks Part 1: An expanded structural geobarometer for anhydrous and hydrous, basic and ultrabasic systems. Contributions to Mineralogy and Petrology, 133: 122–135. https://doi.org/10.1007/s004100050442

Otten, M.T. 1984: The origin of brown hornblende in the Artfjället gabbro and dolerites. Contributions to Mineralogy and Petrology, 86: 189–199. https://doi.org/10.1007/BF00381846

Papike, J.J., Cameron, K.L. & Baldwin, K. 1974: Amphiboles and pyroxenes: characterization of other than quadrilateral components and estimates of ferric iron from microprobe data. Geological Society of America Abstract Program, 6: 1053–1054.

Poldervaart, A. & Hess, H.H. 1951: Pyroxenes in the Crystallization of Basaltic Magma. Journal of Geology, 59/5: 472–489. https://doi.org/10.1086/625891

Poli, G., Christofides, G., Koroneos, A., Trajanova, M. & Zupančič, N. 2020: Multiple processes in the genesis of the Pohorje igneous complex: Evidence from petrology and geochemistry. Lithos, 364–365: 105512. https://doi.org/10.1016/j.lithos.2020.105512

Schmidt, M.W. 1992: Amphibole composition in tonalite as a function of pressure: an experimental calibration of the Al-in-hornblende barometer. Contributions to Mineralogy and Petrology, 110/2–3: 304–310. https://doi.org/10.1007/BF00310745

Sotelšek, T. 2019: Globina kristalizacije pohorskega granodiorita. Diplomsko delo. Univerza v Ljubljani, Naravoslovnotehniška fakulteta, Ljubljana: 67 p.

Spear, F.S. 1981: Amphibole-plagioclase equilibria: an empirical model for the reaction albite

+ tremolite = edenite + 4 quartz. Contributions to Mineralogy and Petrology, 77: 355–364. https://doi.org/10.1007/BF00371564

Stein, E. & Dietl, C. 2001: Hornblende thermobarometry of granitoids from the Central Odenwald (Germany) and their implications for the geotectonic development of the Odenwald. Mineralogy and Petrology, 72: 185–207. https://doi.org/10.1007/s007100170033

Trajanova, M., Pécskay, Z. & Itaya, T. 2008: K-Ar geochronology and petrography of the Miocene Pohorje Mountains batholith (Slovenia). Geologica Carpathica, 59: 247–260.

Vrabec, M., Janák, M., Froitzheim, N. & De Hoog, J.C.M. 2012: Phase relations during peak metamorphism and decompression of the UHP kyanite eclogites, Pohorje Mountains (Eastern Alps, Slovenia). Lithos, 144–145: 40–55. https://doi.org/10.1016/j.lithos.2012.04.004

Yavuz, F. & Döner, Z. 2017: WinAmptb – A Windows program for calcic amphibole thermobarometry. Periodico di Mineralogia, 86: 135–167. https://doi.org/10.2451/2017PM710

Zupančič, N. 1994: Petrološke in geokemične značilnosti pohorskih magmatskih kamnin. Doktorska disertacija. Univerza v Ljubljani, Fakulteta za naravoslovje in tehnologijo, Ljubljana: 126 p.